

Article

Understanding Voltage Behavior of Lithium-Ion Batteries in Electric Vehicles Applications

Foad H. Gandoman ^{1,2} , Adel El-Shahat ^{3,*} , Zuhair M. Alaas ⁴ , Ziad M. Ali ^{5,6} , Maitane Berecibar ^{1,2} and Shady H. E. Abdel Aleem ⁷ 

- ¹ Research Group MOBI—Mobility, Logistics and Automotive Technology Research Centre, Vrije Universiteit Brussel, 1050 Brussel, Belgium
² Flanders Make, 3001 Heverlee, Belgium
³ Energy Technology Program, School of Engineering Technology, Purdue University, West Lafayette, IN 47907, USA
⁴ Electrical Engineering Department, College of Engineering, Jazan University, Jazan 45142, Saudi Arabia
⁵ Electrical Engineering Department, College of Engineering, Prince Sattam Bin Abdulaziz University, Wadi Addawaser 11991, Saudi Arabia
⁶ Electrical Engineering Department, Aswan Faculty of Engineering, Aswan University, Aswan 81542, Egypt
⁷ Department of Electrical Engineering, Valley High Institute of Engineering and Technology, Science Valley Academy, Qalyubia 44971, Egypt
* Correspondence: asayedah@purdue.edu

Abstract: Electric vehicle (EV) markets have evolved. In this regard, rechargeable batteries such as lithium-ion (Li-ion) batteries become critical in EV applications. However, the nonlinear features of Li-ion batteries make their performance over their lifetime, reliability, and control more difficult. In this regard, the battery management system (BMS) is crucial for monitoring, handling, and improving the lifespan and reliability of this type of battery from cell to pack levels, particularly in EV applications. Accordingly, the BMS should control and monitor the voltage, current, and temperature of the battery system during the lifespan of the battery. In this article, the BMS definition, state of health (SoH) and state of charge (SoC) methods, and battery fault detection methods were investigated as crucial aspects of the control strategy of Li-ion batteries for assessing and improving the reliability of the system. Moreover, for a clear understanding of the voltage behavior of the battery, the open-circuit voltage (OCV) at three ambient temperatures, 10 °C, 25 °C, and 45 °C, and three different SoC levels, 80%, 50%, and 20%, were investigated. The results obtained showed that altering the ambient temperature impacts the OCV variations of the battery. For instance, by increasing the temperature, the voltage fluctuation at 45 °C at low SoC of 50% and 20% was more significant than in the other conditions. In contrast, the rate of the OCV at different SoC in low and high temperatures was more stable.

Keywords: battery management system; electric vehicles; lithium-ion batteries; open-circuit voltage; state of charge; state of health



Citation: Gandoman, F.H.; El-Shahat, A.; Alaas, Z.M.; Ali, Z.M.; Berecibar, M.; Abdel Aleem, S.H.E. Understanding Voltage Behavior of Lithium-Ion Batteries in Electric Vehicles Applications. *Batteries* **2022**, *8*, 130. <https://doi.org/10.3390/batteries8100130>

Academic Editor: Carlos Ziebert

Received: 22 July 2022

Accepted: 15 September 2022

Published: 20 September 2022

Publisher's Note: MDPI stays neutral with regard to jurisdictional claims in published maps and institutional affiliations.



Copyright: © 2022 by the authors. Licensee MDPI, Basel, Switzerland. This article is an open access article distributed under the terms and conditions of the Creative Commons Attribution (CC BY) license (<https://creativecommons.org/licenses/by/4.0/>).

1. Introduction

Due to announcing many electric vehicles (EVs) in 2020 in the EU, many companies and firms have invested in gaining more market share in this hot area. One of the essential components of future transportation systems is batteries [1]. Li-ion batteries have been introduced as the leading alternative for providing electric energy for E-mobility applications' power train. Lithium-ion batteries may be the best option for powering an EV in modern transportation systems due to their high energy density, high energy efficiency, long cycle life, and low weight [2]. Lithium-ion battery-powered EVs can classically travel a certain distance only before their batteries need to be replaced. A battery charging system and a new battery control strategy are necessary for EV applications because of the limited usable range.

Different rechargeable batteries have been introduced in the literature, and many have been given attention for operation in EVs. Other types of Li-ion battery cells frequently use Carbon (C) and Lithium Titanium Oxide (LTO) anode materials, and Nickel-Manganese-Cobalt (NMC), Lithium-Ion-Phosphate (LFP), Nickel-Cobalt-Aluminum-Oxide (NCA), and Lithium-Ion Manganese Oxide (LMO) cathode materials. Besides, Lithium-Sulfur (Li-S), due to its advantages, is going to be a new set of Li-ion batteries, as illustrated in Figure 1 [3].

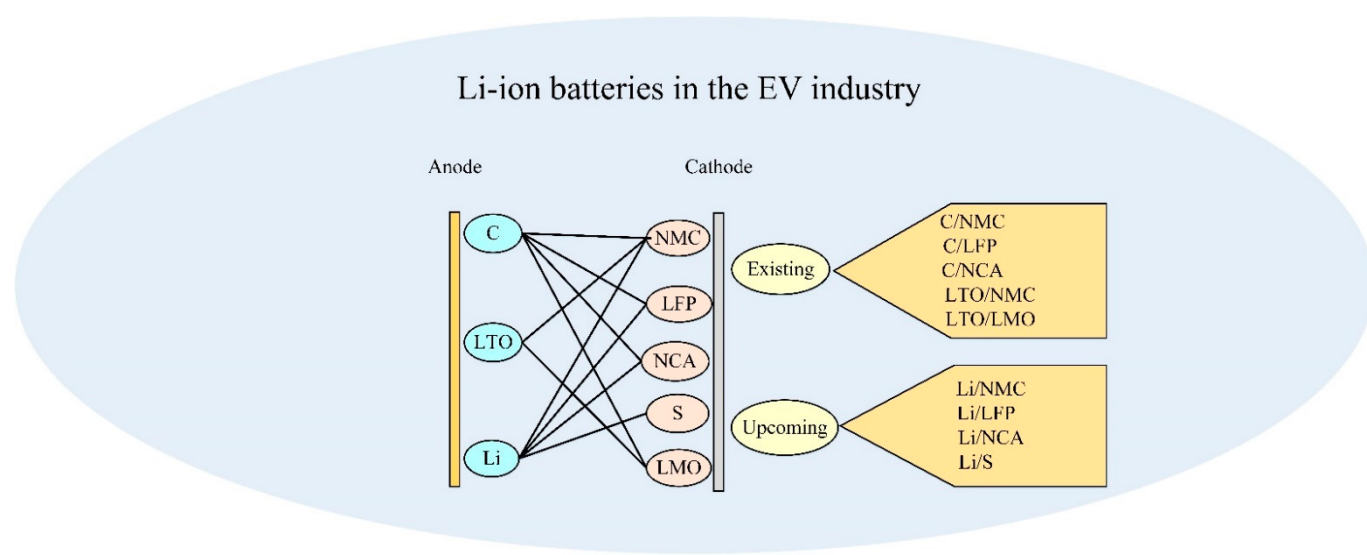


Figure 1. Li-ion batteries in the automotive industry.

The battery management system (BMS) in a Li-ion battery pack is critical [4,5]. Controlling discharging and charging, voltage monitoring, battery balancing, temperature management in cells and battery packs, problems detection and assessment, communication and networking, and system dependability are all responsibilities of the BMS [6,7]. The BMS system's fundamental, hardware, and software aspects significantly affect its overall performance [8,9]. Currently, Li-ion battery pack BMS comprises monitoring of battery cells, input/output current and voltage monitoring, charging/discharging control, estimations of the state of charge (SoC) [10,11], the state of health (SoH) [12], and the state of function [13], as well as battery protection [14,15] and cell balancing and equalization [16].

Li-ion batteries, due to aging, provide metallic lithium plating and the lithium dendrite and solid electrolyte interphase layer, which may lead to dangerous failures if operated under specific conditions, such as overcharging, over-discharging, or running at a low temperature [17]. As a result, BMS fault detection and diagnostic functions are crucial for Li-ion battery-driven systems, particularly for high-power applications. Improving BMS and SoH estimation algorithms for battery system fault avoidance and lifetime improvement based on the safe operating envelope (SOE) assessment are vital functions that play an essential role in battery performance over time. Additionally, optimization of power flow and grid capacity evaluation in the different SoC windows and SOP of the battery system in terms of fast and high-power charging solutions in EVs are the main challenges for electricity utilities [18]. Thus, the development of the multi-domain novel platform (digital twin) to provide a comprehensive overview regarding battery aging key aspects, such as SoH, SOE, and SoC estimation based on the non-invasive diagnostic and post-mortem degradations techniques, impacts the fast-charging solutions on the grid and plays a vital role in the E-mobility battery strategy roadmap challenges. Additionally, the development of the multi-domain novel platform to virtually model the electrical grid and the operational demonstrators with superfast charging capabilities for evaluation of the short and long impact of the superfast charging on the grid [19,20] (power quality, grid capacity, energy management, etc.) will be valuable for the EVs, chargers, and grid suppliers in all the world.

Many research studies were conducted to advance a precise, robust, reliable, and easy-to-use fault diagnostic method. The importance of creating an efficient system of fault diagnostics for the evolution of Li-ion battery-powered systems was studied in ref. [13]. The authors in ref. [21] presented a detailed synopsis of the failure process of Li-ion batteries and potential remedies in a state-of-the-art review article. An overview of alternative problem diagnostic techniques for Li-ion batteries was presented in ref. [22].

In this context, estimating the SoC, SoH, and open-circuit voltage (OCV) [23] is essential in improving the Li-ion batteries' control and lifetime [24]. The SoC estimate of Li-ion batteries tries to verify a battery's remaining capacity throughout a charge-discharge cycle, preventing the battery from overcharging and over-discharging [3]. The purpose of the SoH calculation is to anticipate the remaining usable life of charge-discharge cycles, determining whether Li-ion batteries need to be replaced. On the other hand, the SoH of the battery is characterized by slow-changing properties like capacity fading and resistance rising, and it fluctuates with cycles, necessitating long-term monitoring [25].

In ref. [26], the SoC estimation of Li-ion batteries relying on battery models and the advantages and disadvantages of the estimation techniques were discussed. Also, the erroneous causes influencing the SoC estimate were investigated in ref. [27], but the review of the estimation technique was brief. The authors in ref. [28] highlighted the fundamental problems and summarized the live SoC estimate based on the family of Kalman filter (KF) algorithms. Rather than model-based SoC assessment, the authors in ref. [29] focused on data-driven estimation approaches of SoC for Li-ion batteries used in EV applications. The authors in ref. [30] divided the battery SoH estimates between experimental and model-based techniques but did not detail each estimating method's merits and demerits.

In this regard, the BMS concept, SoH and SoC methods, and battery fault detection methods have been investigated as crucial aspects of the control strategy of Li-ion batteries for assessing and improving the system's reliability [29,31–35]. Moreover, for a clear understanding of the voltage behavior of the battery, the OCV variation at three ambient temperatures and three different SoC percentages have been investigated. The experimental results obtained show that changing the ambient temperature impacts the OCV variations of the Li-ion battery.

The rest of the work is organized as follows: A brief overview of the battery control strategy based on the BMS operation is presented in Section 2. Section 3 investigates a case study based on the voltage variation of the battery at various ambient temperatures over time. Discussion of the results is presented in Section 4. The conclusion and future works are presented in Section 5.

2. Battery Management System (BMS)

EVs have a BMS that controls and monitors an EV's battery system [36,37]. The BMS maintains battery safety and dependability, improves efficiency, extends battery life, and boosts EV range. A battery system is essential since a single cell has limited capacity and voltage. A battery system comprises several cells connected in series, parallel, or a mix of both to achieve a specific capacity or voltage level. The BMS is responsible for estimating battery states and characteristics, preventing overcharging, over-discharging, thermal runaway, and battery inconsistencies [27].

Regarding hardware implementation, the BMSs have five primary tasks to attain an optimal and efficient operation [13]—battery parameter acquisition, battery system balancing, battery information management, battery thermal management, and battery charge regulation. Some of the combined features of battery storage in the BMS are given as follows:

- Expenditure consists of producing, reparation, function, and transforming expenditure;
- The life cycle is determined by charging or discharging;
- The power supply is determined by the charging or discharging amount and energy storage amount;

- Security determines the safety or hazardous elements because of the functional operating temperature.

BMS may be simple or complicated, and they can use various technologies to fulfill their primary goal (taking care of the battery). In general, there are four topologies for BMS in EVs. Table 1 describes the merits and demerits of these topologies. The systems may be classified depending on how they are deployed and work throughout the battery pack's cells or modules while keeping topologies in mind.

Table 1. Merits and demerits of four topologies of BMS in EV applications.

BMS Type	Definition	Merits	Demerits
Centralized	The battery pack has one central BMS, and all the battery packages are directly connected to the central BMS	Because there is just one BMS, it is more compact and tends to be the most cost-effective	The BMS requires many ports to connect with all battery packages because the batteries directly link to the BMS
Modular	The BMS is divided into numerous replicated modules, each with its dedicated bundle of wires and connects to a battery stack's neighboring allocated section	Troubleshooting and maintenance are simplified because of the inherent flexibility, and expansion to bigger battery packs is simple	The disadvantage is that total expenses are somewhat more significant, and unnecessary functionality may be duplicated depending on the program
Subordinate	Similar to the modular architecture in concept, however, in this instance, the slaves are limited to just relaying measurement data, while the master is devoted to calculation, control, and external communication	Because the slaves' functionality is often more straightforward, there is likely less overhead and fewer unwanted features, and the expenses may be cheaper than with a modular BMS	The disadvantage is as the modular BMS
Distributed	The electrical hardware and software are housed in modules that connect to the cells through bundles of wires. All the electrical gear for a distributed BMS is housed on a control board mounted directly on the monitored cell or module	Most wiring is reduced to a few sensor wires and communication cables between nearby BMS modules. In addition, each BMS is more self-contained, allowing it to conduct calculations and communications as needed	Troubleshooting and maintenance might be complex with this integrated form. Because there are more BMSs in the total battery pack system, costs are likewise higher

The BMS has some tasks that are presented as follows:

- Cell monitoring: It consists of current, voltage, and temperature situations;
- Battery safety: To provide the security of the battery and eliminate it from dangerous situations;
- SoC evaluation: SoC is a metric of the existing charge storage in the battery that shows the entire status of battery charging;
- SoH evaluation: SoH is a significant metric of battery operation features. It forecasts the quantity of charging and discharging duration;
- Cell regulation: It consists of various arrangements of battery cells to provide suitable functions to the battery system.

Furthermore, as depicted in Figure 2, which shows a detailed picture of the BMS features configuration, the BMS has some elements that are outlined as follows:

- CAN-bus component, which is applied for relating with control elements;
- The DC/DC component converts the power source into the power supply;
- The battery current evaluation component is applied for calculating the charging and discharging current situation;
- A battery voltage evaluation component is used to calculate the voltage situation;

- A temperature evaluation component is applied to check the case of selected cells;
- The data flash memory component is applied for recording data for evaluation.

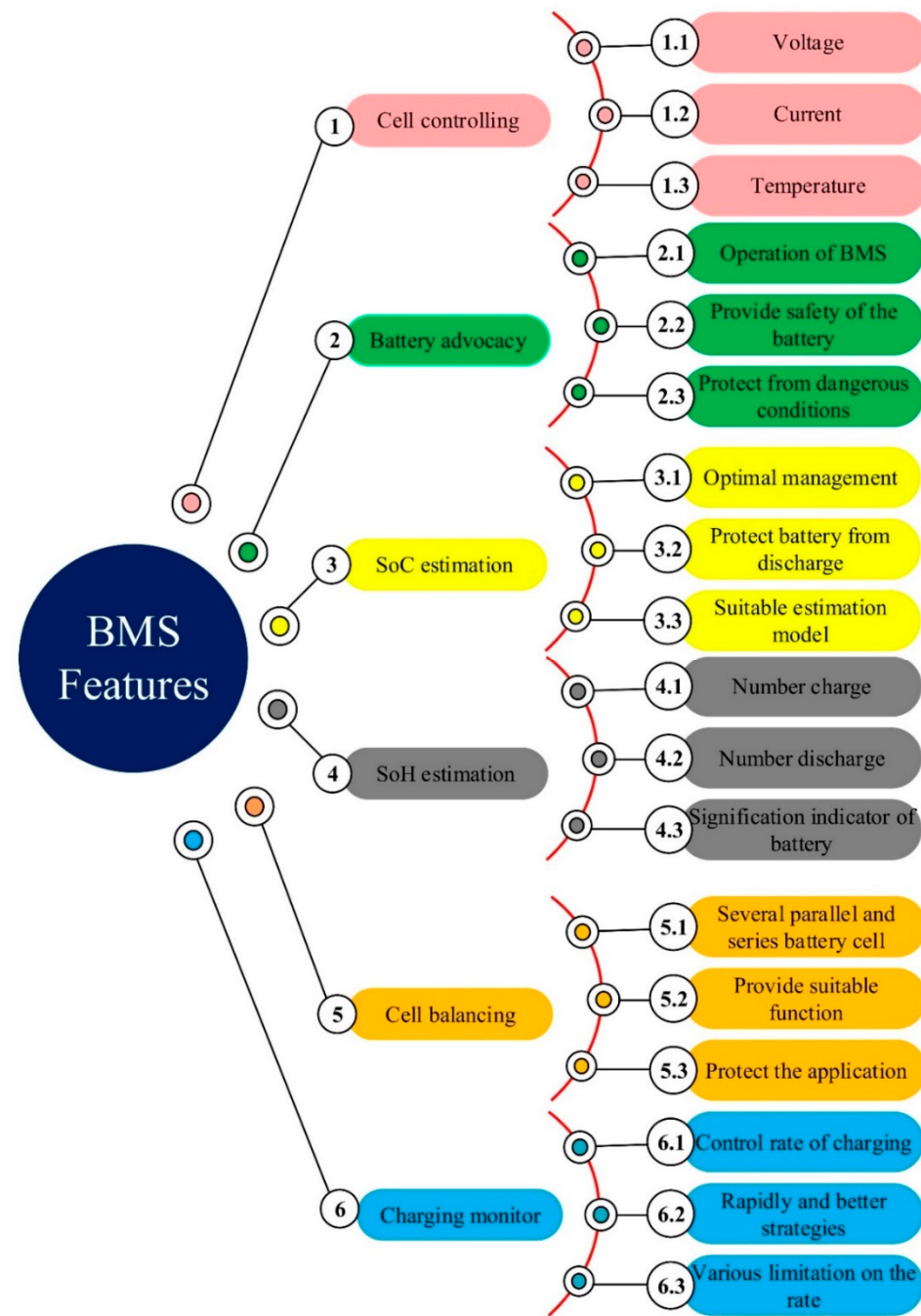


Figure 2. BMS features.

Finally, all components of BMS must be related to the selected control element to operate correctly in an efficient manner.

3. Investigation of Voltage Variations of a Li-Ion Battery under Different Temperatures (OCV Test)

Figure 3 illustrates the workflow of the case study used to investigate the OCV variation of a Li-ion battery (3Ah Nickel-Manganese-Cobalt (NMC) battery) under different ambient temperatures during the lifetime of the Li-ion battery. Based on the proposed workflow, the battery needs to be cycled under three ambient temperatures, 45 °C, 25 °C,

and 10 °C, at a specific rate so that the SoH of the battery reaches 80%. Afterward, the data collected in the test center will be investigated to understand better the OCV variation of the battery over time.

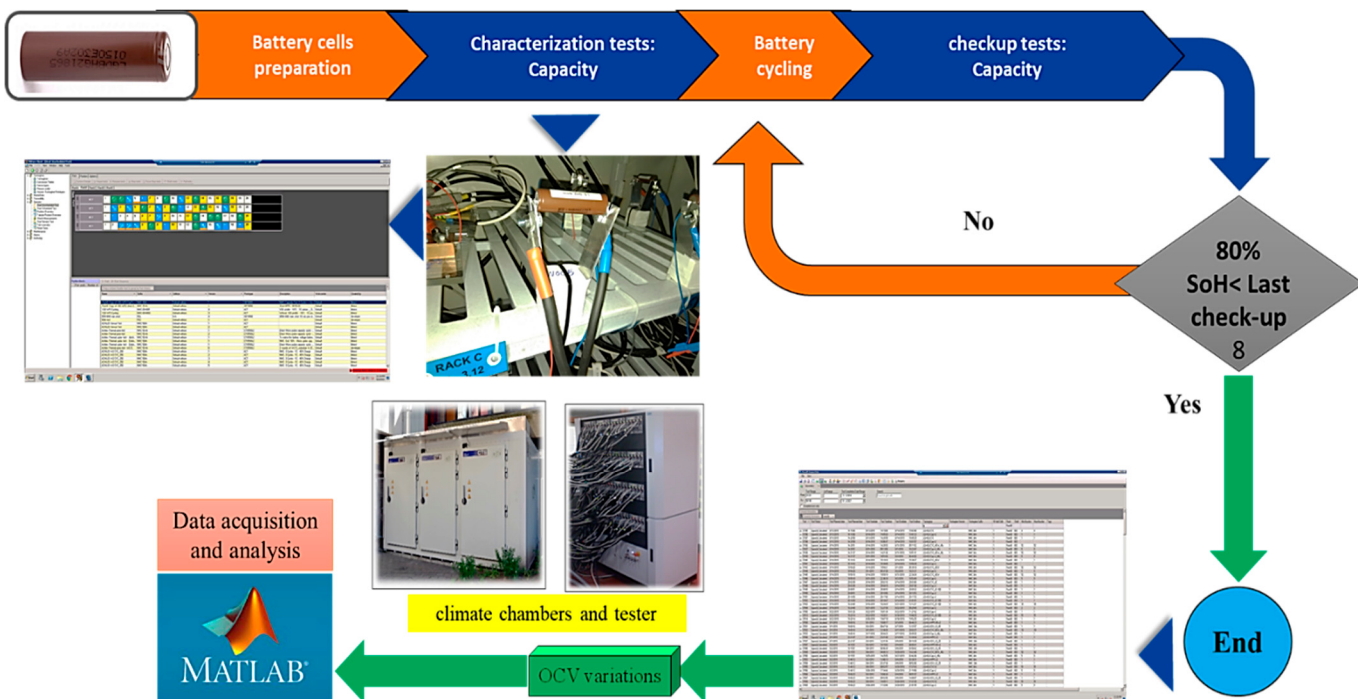


Figure 3. Proposed workflow of the case study used to investigate the OCV variation of a Li-ion battery.

OCV provides the cell's open-circuit voltage at various SoC levels (IEC 62660-1). The OCV curve, measured at different temperatures, points to the status of a battery (charge and discharge) in the studied case. In this characterization test, as shown in Figure 4, the cell is initially charged at 100% SoC with a C/2 current rate, where the C-rate governs the electric current to charge and discharge a battery in a specified period completely. A capacity discharge test was executed before the experiment to determine the total discharge capacity of each cell at different temperatures (10 °C, 25 °C, and 45 °C).

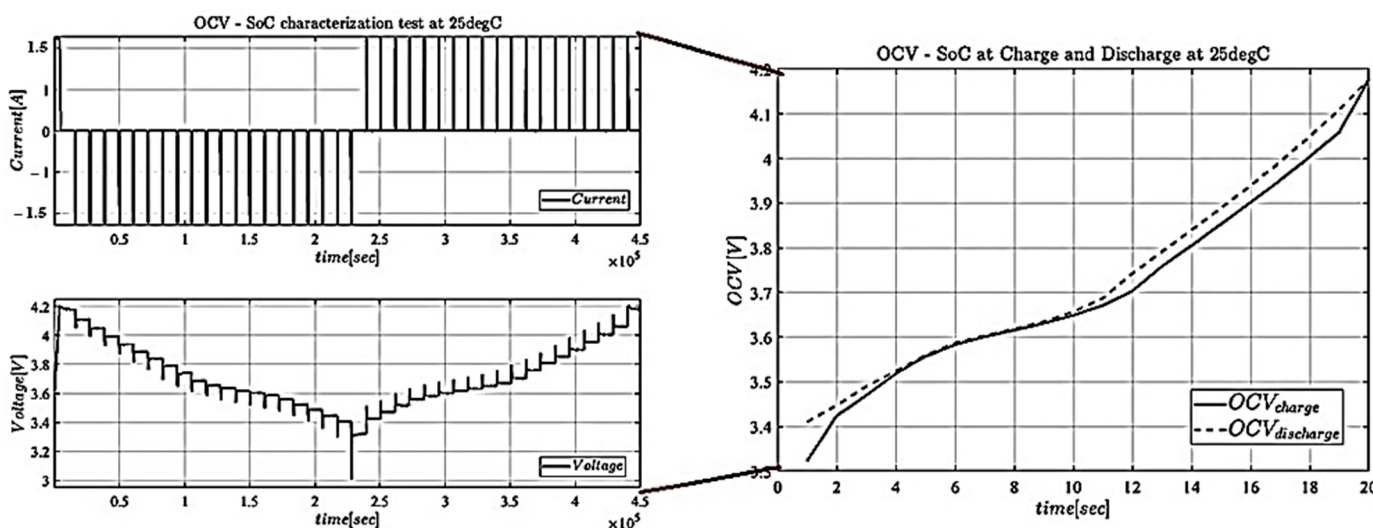


Figure 4. Implemented OCV test to the 3Ah NMC Li-ion battery at 25 °C.

In this test, the cell rested for 3 h, and the OCV was calculated from the last voltage point. Then it was discharged with $C/2$ for a 5% reduction in the total discharged capacity, rested for 3 h, and the OCV for the revised SoC was measured. This procedure continued until the cell reached its safety limit ($V_{min} = 3$ V), where the final value of the OCV was measured for a 5% SoC. The last number is the starting point for the charging OCV, which continues similarly but with a positive current until the upper safety limit (V_{max}) of the battery cell is reached.

Figure 4 depicts an experimental result at a temperature of 25 °C. It is worth noting that the OCV during charge and discharge has similar behavior and values relying on the findings. Additionally, the OCV curves for all tests emphasize the effect of temperature on OCV values.

As can be noticed, the temperature has no remarkable influence on the NMC cell's OCV behavior. In this experiment, the rate of OCV at the above temperatures was investigated in each check-up for 80% SoC, 50% SoC, and 20% SoC. In this investigation, the rate of the OCV during the discharge of the battery was considered.

4. Results and Discussion under Charge–Discharge Standard Test Protocols (STPs) at Different Temperatures

Figures 5–7 explore the OCV at different temperatures under charge–discharge STPs at 80% SoC, 50% SoC, and 20% SoC during the lifetime of the Li-ion battery. The behavior of the OCV during the life cycle of the batteries was more stable at 25 °C than among other conditions. The ambient temperature, internal resistance, and the anode side's structure to store the lithium amount remained more uniform at 25 °C, 10 °C, and 45 °C, respectively. Due to the high temperature of the environment, the OCV behavior at 45 °C has more fluctuations than in other situations. The results, in this case, showed that the battery voltage at 20% SoC was more unbalanced than elsewhere due to being in the knee area.

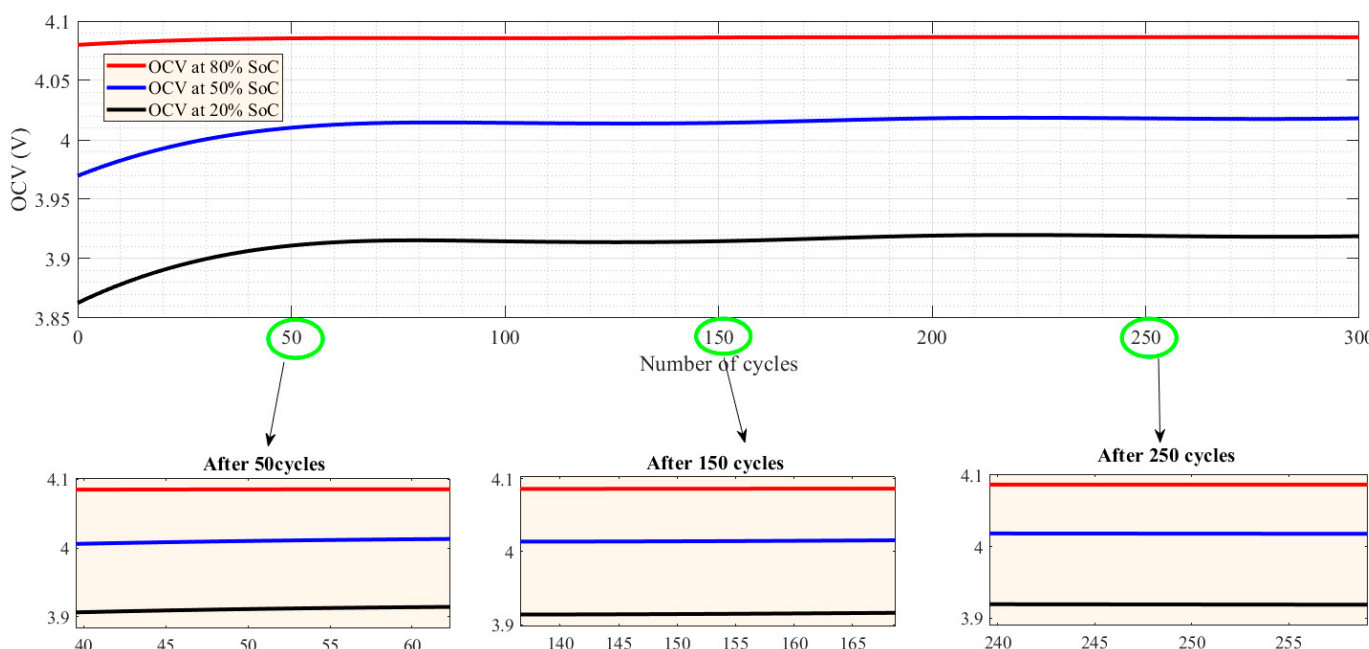


Figure 5. OCV pattern at 25 °C under charge–discharge STPs after 300 cycles during the lifetime of the 3Ah NMC Li-ion battery.

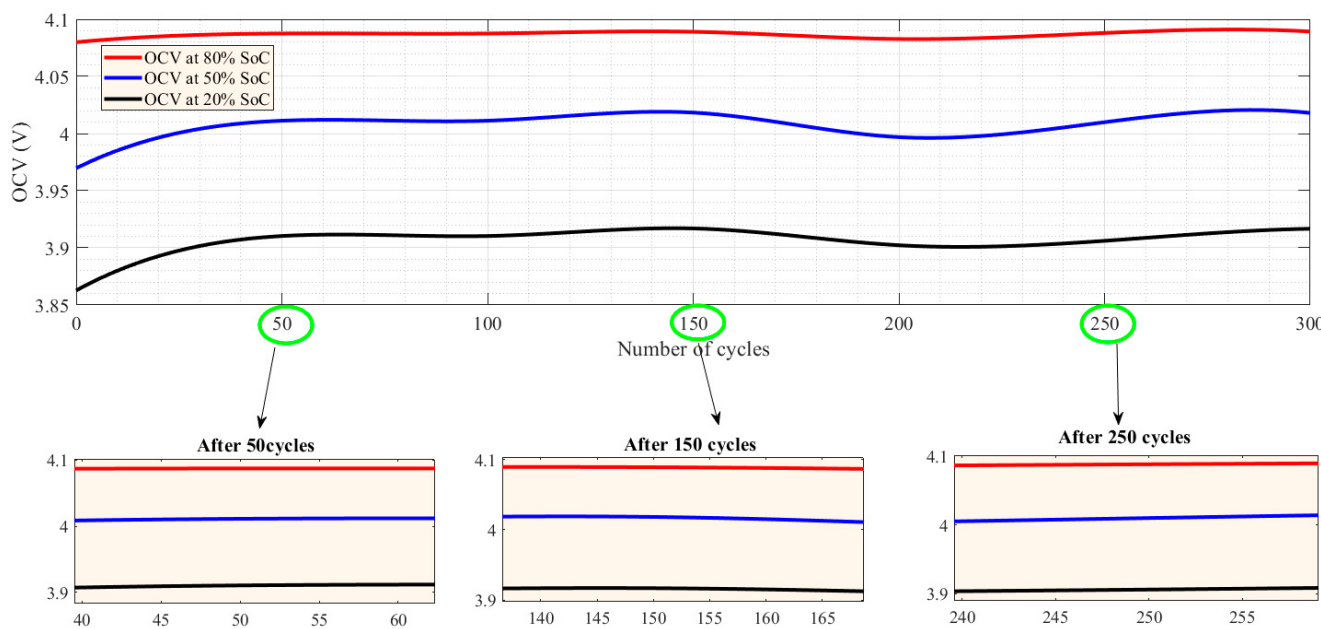


Figure 6. OCV pattern at $45\text{ }^{\circ}\text{C}$ under charge–discharge STPs after 300 cycles during the lifetime of the 3Ah NMC Li-ion battery.

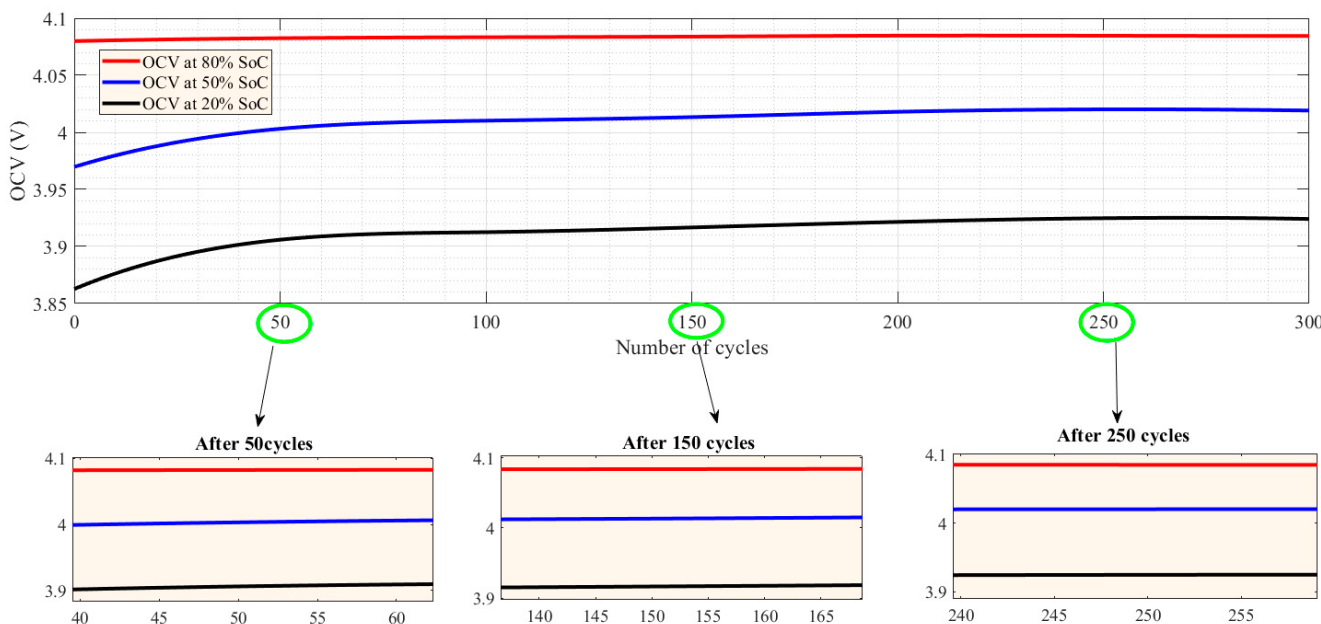


Figure 7. OCV pattern at $10\text{ }^{\circ}\text{C}$ under charge–discharge STPs after 300 cycles during the lifetime of the 3Ah NMC Li-ion battery.

The OCV distribution at 20% SoC, 50% SoC, and 80% SoC at different temperatures and under charge–discharge STPs is depicted in Figure 8. It comprises three chief parts: the right side of Figure 8 illustrates the OCV variations over time, the bottom part (base) represents the number of the check-up tests (OCV via SoC tests), and the left side of the suggested test illustrates the number of the degradation conditions.

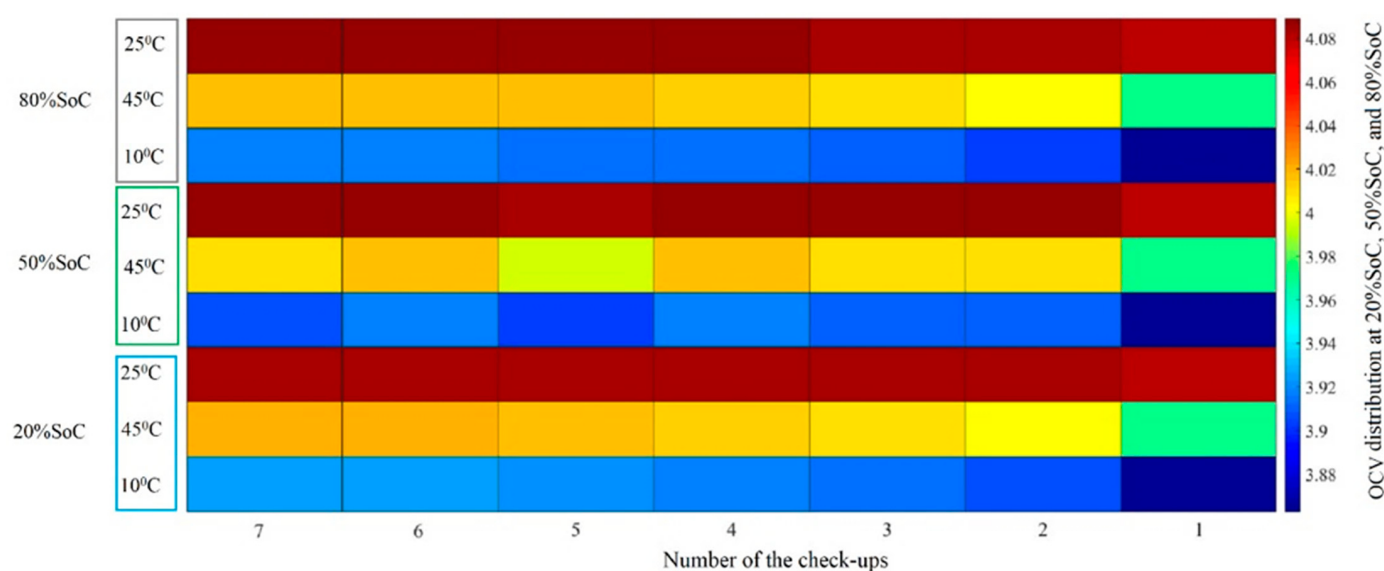


Figure 8. OCV distribution at different SoC percentages under STPs during the lifetime of the battery.

Further, we considered three main temperatures as different conditions of degradation to provide a broad view of the behavior of the battery capacity in the room, low and high temperature. Each temperature area was investigated by relying on the stabilization area of 80% SoC in this work, 50% SoC (linear region), and 20% SoC (knee area). Based on the results, battery OCV variation was at 45 °C for 20% SoC and 50% SoC.

However, the stable conditions regarding OCV were at 10 °C and 25 °C for 80% SoC. The Li-ion does not move through the electrolyte uniformly and in a straight path. Thus, there are fluctuations in OCV during the lifetime of the battery. As depicted in Figure 8, more instability (fluctuation) can be observed at high temperatures compared with low temperatures as the lithium-ions move in a more non-uniform way at high temperatures. However, the amount of lithium that has been stored in the active material particle is dependent on high kinetic energy, and this issue increases the rate of the voltage at the end of the life at 45 °C more than in other conditions.

Figures 9–13 illustrate the OCV under various charge–discharge STPs at 80% SoC, 50% SoC, and 20% SoC during the lifetime of the battery at 25 °C temperature to comprehensively overview the OCV distribution.

The distribution of the OCV at different temperatures is presented in Figure 14. According to the results, the trend of the OCV after 2C was described. We considered five discharge C-rates as degradation conditions for providing multi-domain behaviors at 25 °C and high and low discharge C-rates. Moreover, each temperature area was investigated by relying on the stabilization area of SoC (80% SoC in this work), linear region of SoC (50% SoC in this work), and knee area of SoC (20% SoC in this work). Since there is a certain amount of active battery material in which lithium is gradually involved during electrochemical reactions over the battery's life, the battery voltage slightly increases during cycling.

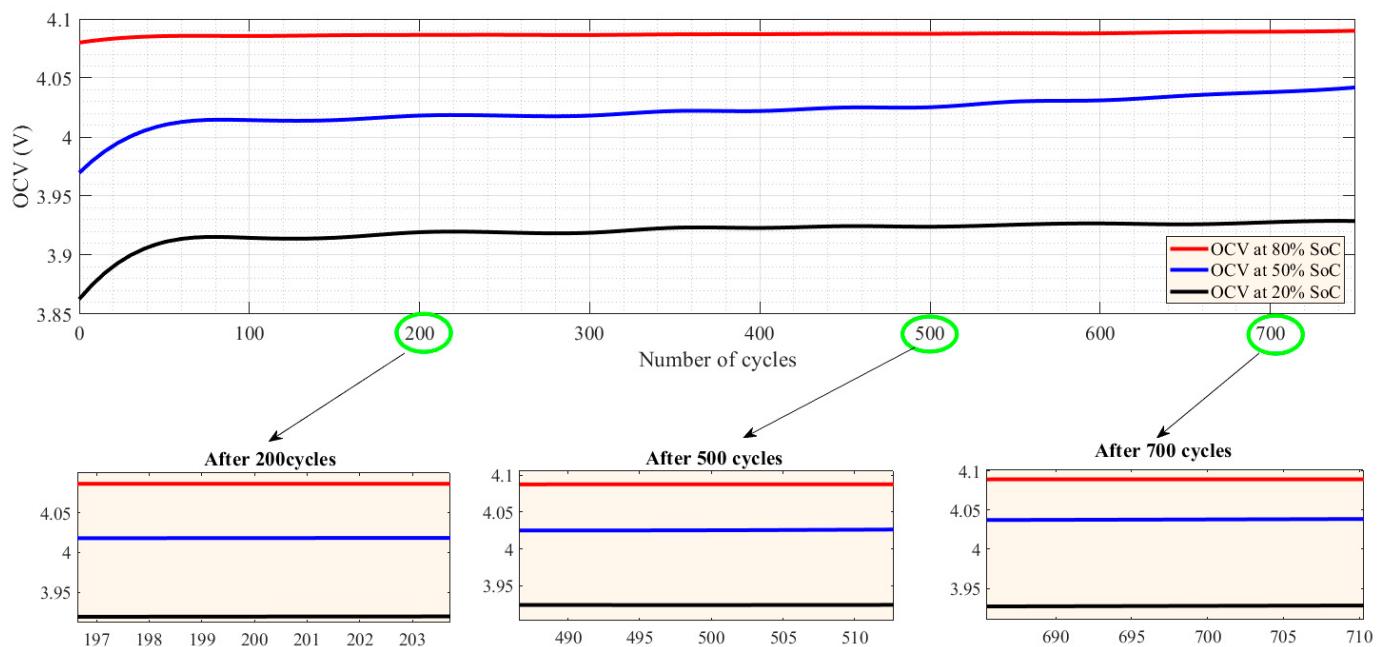


Figure 9. Comparison of the OCV pattern at 25 °C under C/2 charge and C/5 discharge test conditions.

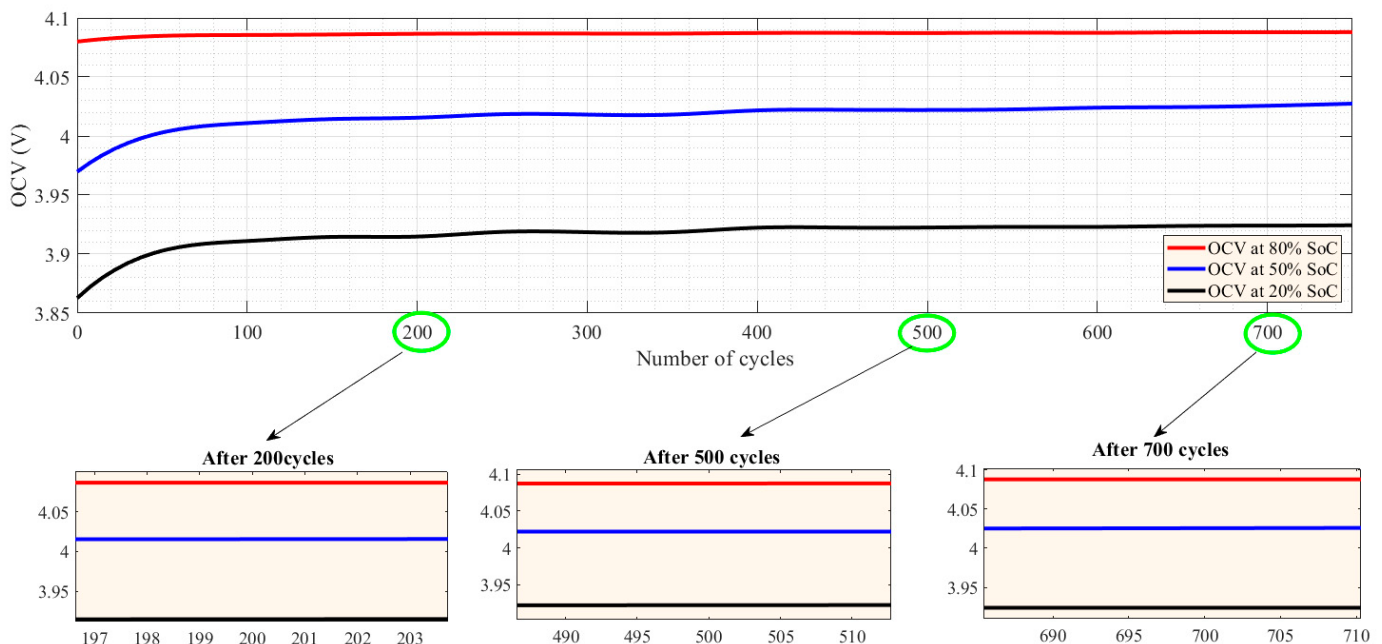


Figure 10. Comparison of the OCV pattern at 25 °C under C/2 charge and 1 C discharge test conditions.

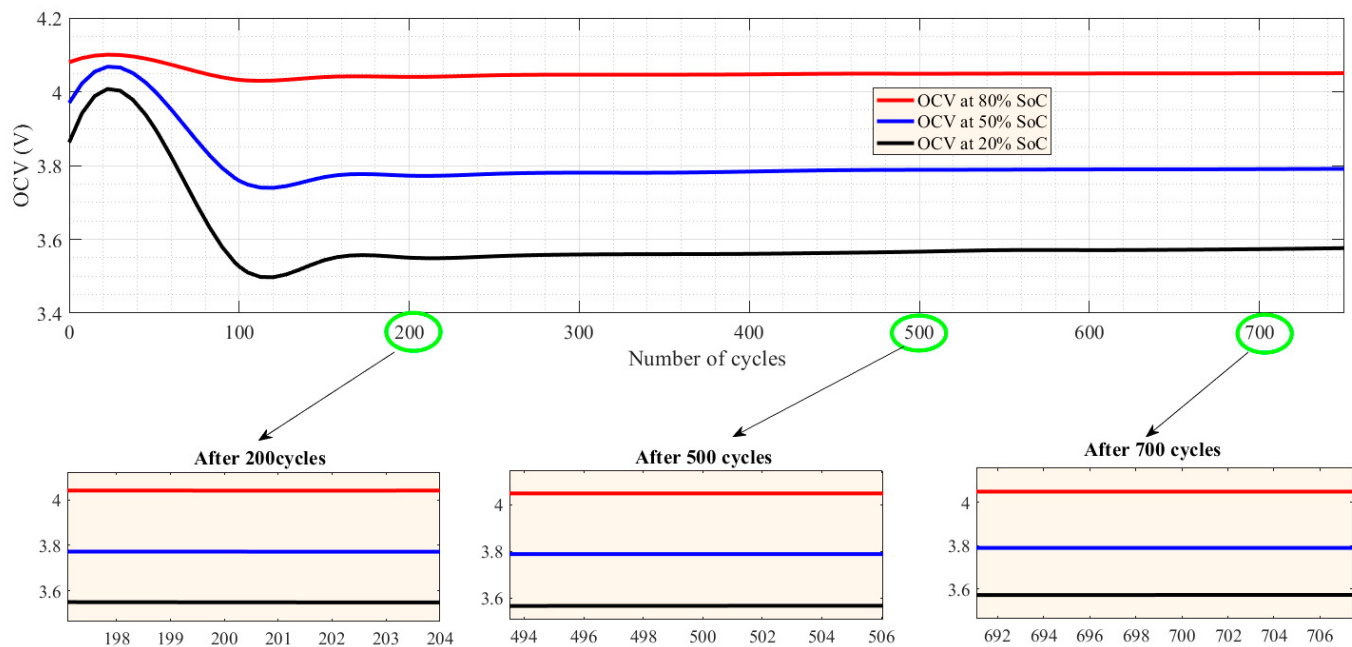


Figure 11. Comparison of the OCV pattern at 25 °C under C/2 charge and 2 C discharge test conditions.

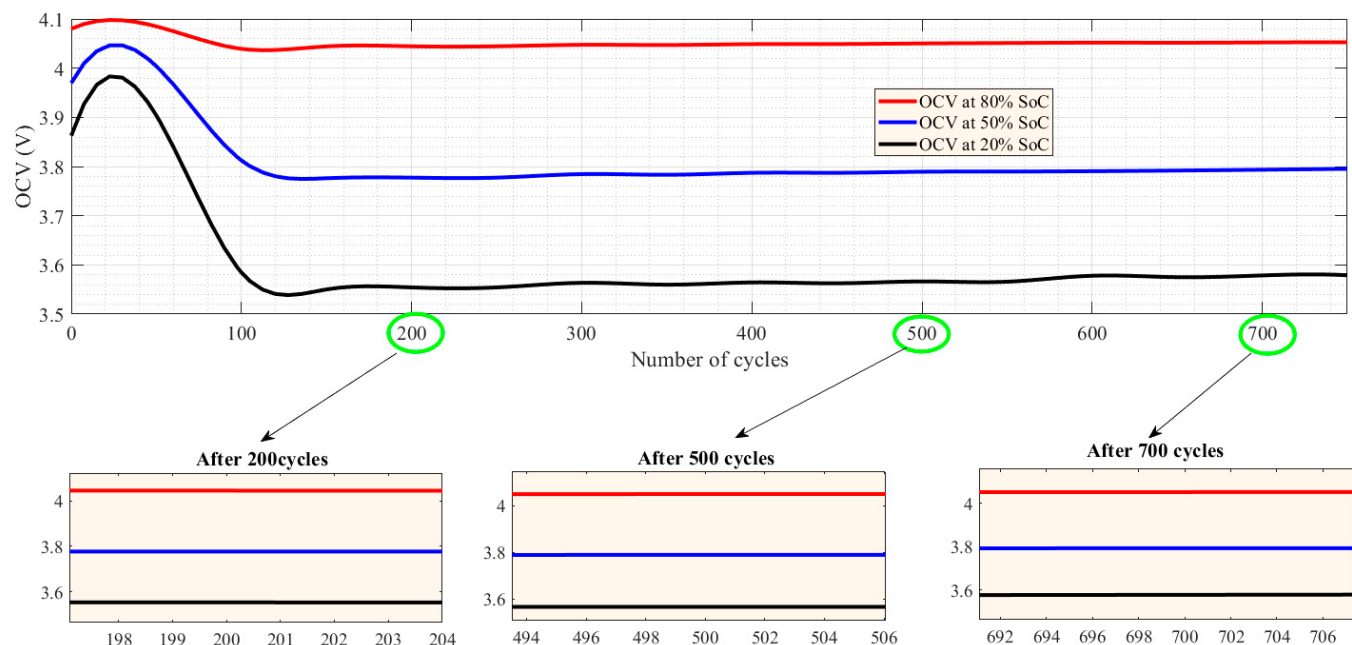


Figure 12. Comparison of the OCV pattern at 25 °C under C/2 charge and 3C discharge test conditions.

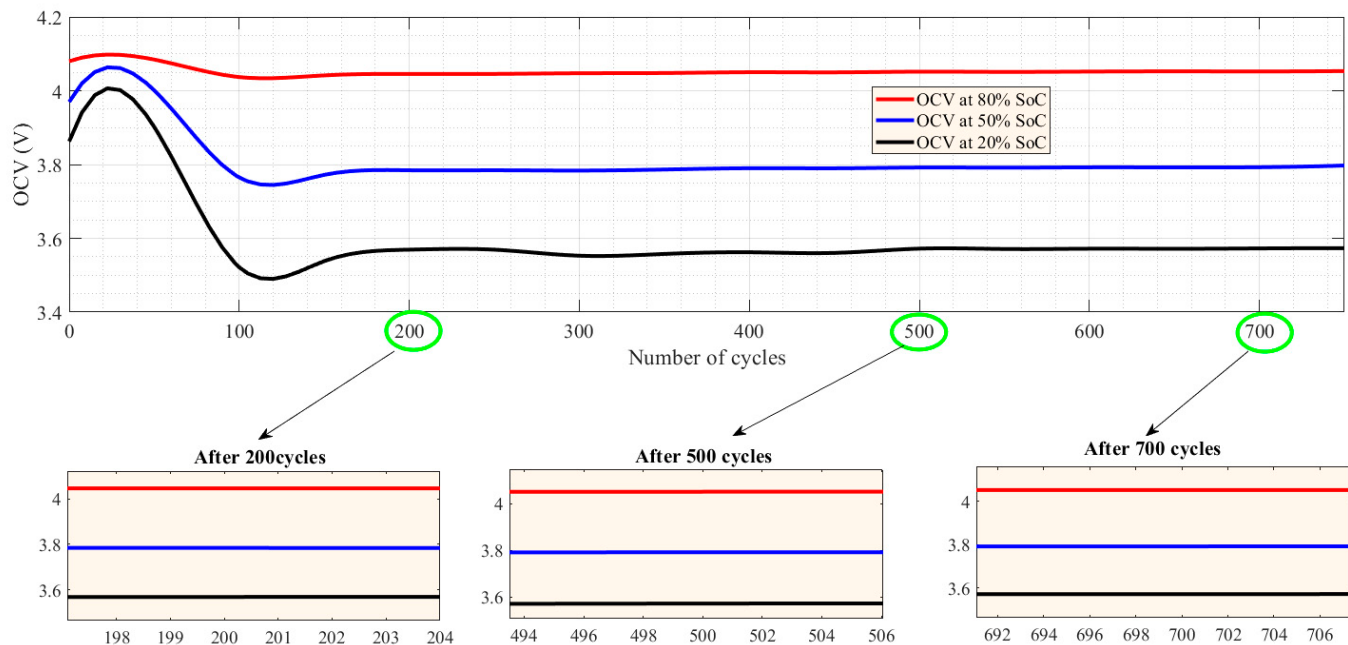


Figure 13. Comparison of the OCV pattern at 25 °C under C/2 charge and 4C discharge test conditions.

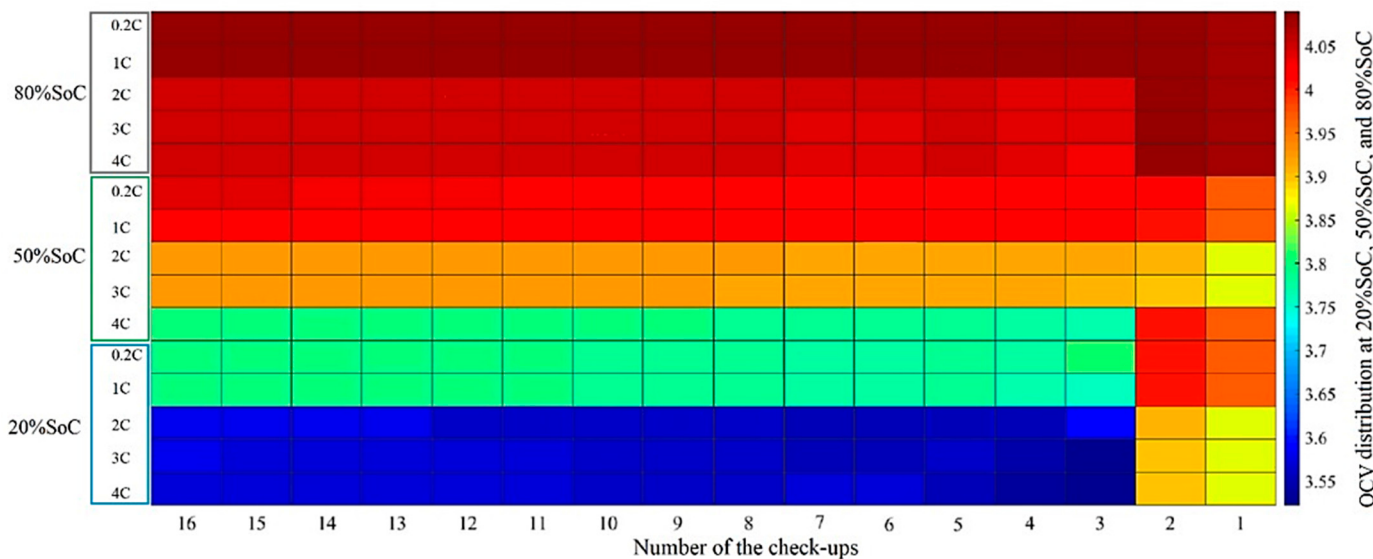


Figure 14. OCV distribution at different SoC percentages at 25 °C under different test conditions.

Under different discharge current test protocols, the OCV distribution results showed that the OCV drops when the C-rate was $\geq 2\text{C}$ during the lifetime of the battery. In other words, with an increasing C-rate, the level of the OCV decreases slightly; this effect appeared most distinctively for medium and low SoC percentages.

Figures 15–17 show the OCV at different temperatures and under other charge-discharge STPs during the lifetime of the battery at 80% SoC, 50% SoC, and 20% SoC, 2C, to investigate the alteration of OCV at 45 °C. Additionally, the effect of the high discharge C-rate at 80% SoC and 20% SoC was less and more during the lifetime of the battery, respectively.

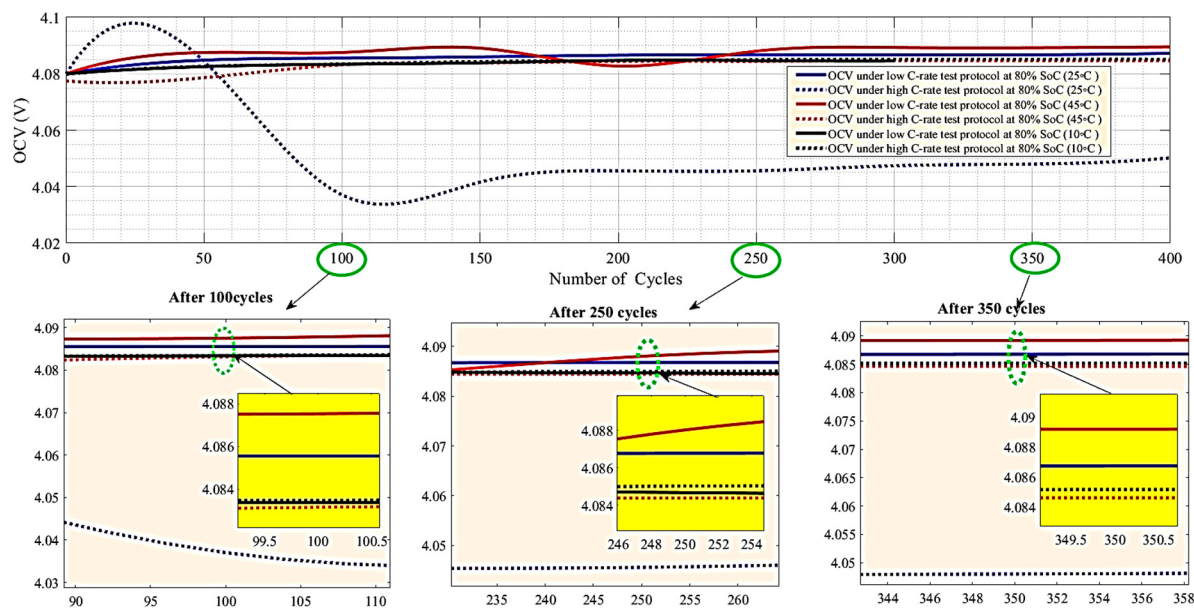


Figure 15. Behavior of OCV at 10 °C, 25 °C, and 45 °C under high and low discharge tests during the lifetime of the battery at 80% SoC.

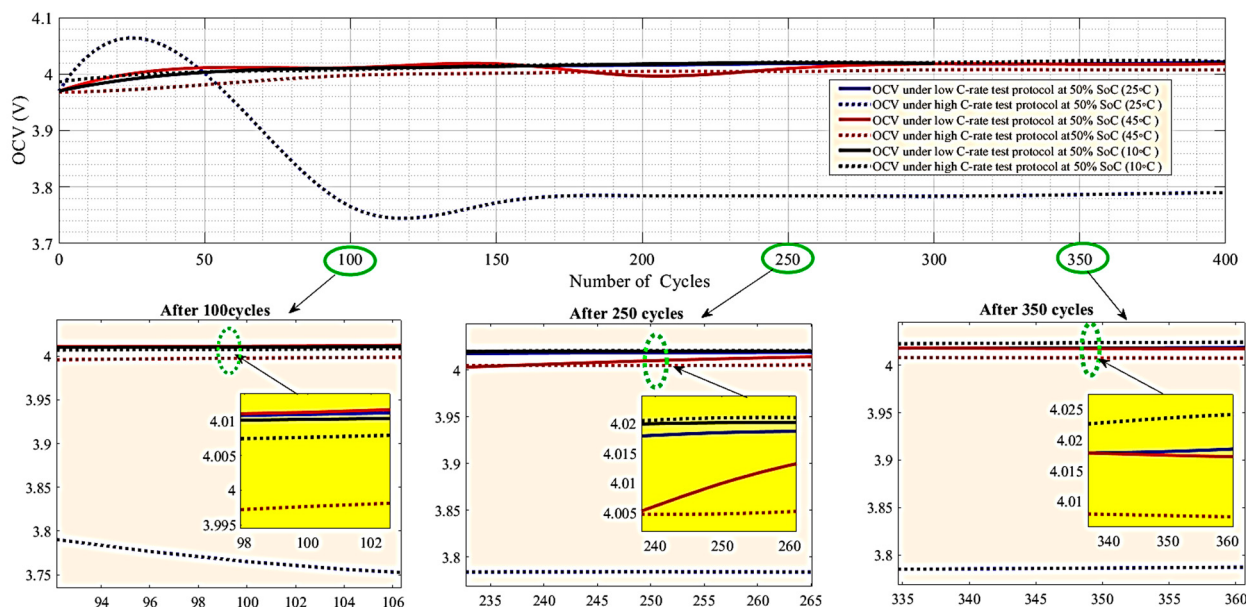


Figure 16. Behavior of OCV at 10 °C, 25 °C, and 45 °C under high and low discharge tests during the lifetime of the battery at 50% SoC.

Evidently, from the results shown in Figure 16, the rate of the OCV at different temperatures under STP in charging and C/5 discharge at 80% SoC was greater than in other conditions after 100 cycles. However, the rate of the difference during the lifetime of the batteries was closer to each other, but still, the rate of the OCV at the same status was higher than in the other conditions.

Figure 17 shows the rate of the OCV at different temperatures under the standard charge test, and C/5 discharge test condition at 50% SoC was greater than the other conditions after 100 cycles. Moreover, the difference rate fluctuates, but the OCV at the same status was still higher than in other conditions. Figure 18 shows that the OCV at the three temperatures and under standard charge and 4C discharge test condition at 20% SoC was lesser than other conditions after 100 cycles. Moreover, the rate of the OCV at 10 °C

and under standard charge and 4C discharge test at 20% SoC was greater than the other conditions after 700 cycles.

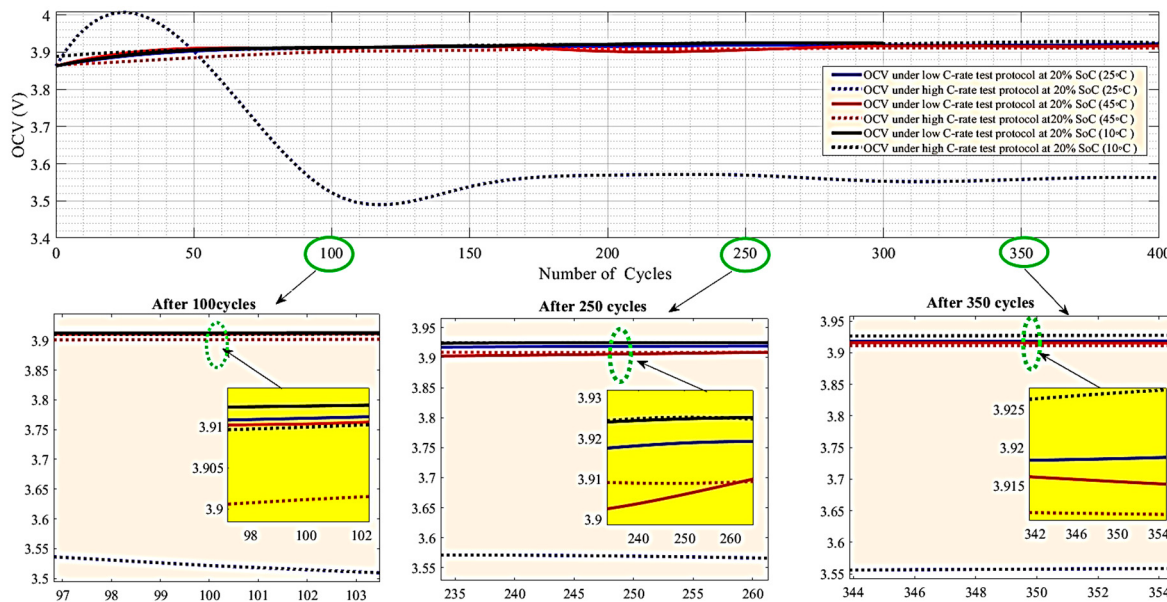


Figure 17. Behavior of OCV at 10 °C, 25 °C, and 45 °C under high and low discharge tests during the lifetime of the battery at 20% SoC.

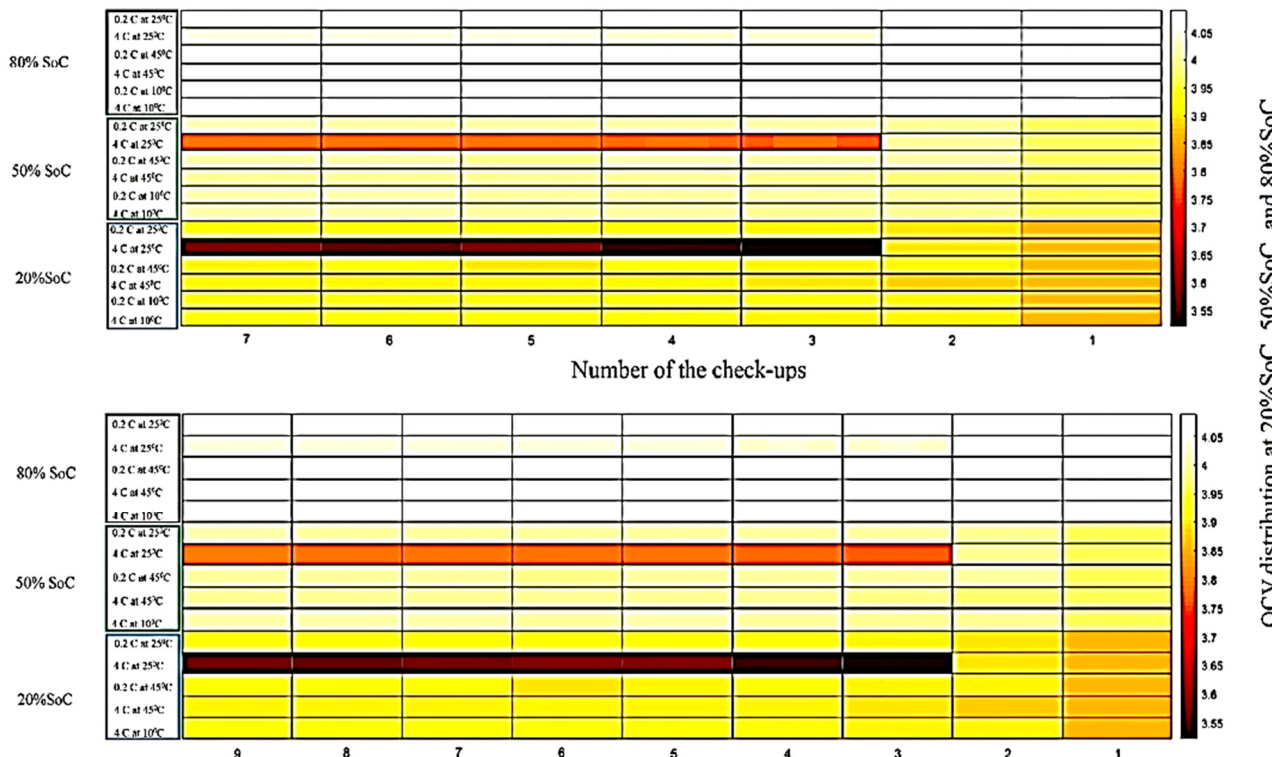


Figure 18. Behavior of the OCV at different SoC percentages under high and low discharge test conditions during the lifetime of the battery.

The OCV distribution is depicted in Figure 18 to broadly overview OCV distribution at different SoC percentages and varying temperatures under various charge and discharge test conditions. At a low C-rate and 10 °C, the rate of the SoH is lower than 80%. Thus, the figured-out distribution splits into two leading figures. Each one comprises three key

parts—OCV variations over time, the number of check-up tests (OCV via SoC tests), and the number of degradation conditions. Three domains of C-rate discharge and temperature (high and low temperatures) have been assumed as conditions of degradation to provide a broad overview of multi-domain discharge current and high and low temperatures conditions.

According to the results, battery OCV variation was greater than in other conditions at 25 °C for 20% SoC and 50% SoC. However, the stable conditions regarding OCV were at 10 °C and 45 °C for 80% SoC. Thus, the change in the temperature does not affect the OCV more at 80% SoC.

Additionally, by increasing the C-rate to 10 °C and 45 °C, the rate of the OCV was slightly increased over time. The high C-rate did not significantly impact the OCV variation at 10 °C and 45 °C. It should be noted that by increasing the C-rate and considering the same internal resistance for all conditions, the rate of the internal heat differs among the conditions. The rate of intramolecular heat impacts the intramolecular path between anode and cathode. Thus, the rate of lithium ions, which are computed and stored in the activities material layer on the anode and cathode sides, differs under a high C-rate test.

Finally, internal heat generation, environment temperature, SoC, and internal resistance are key factors that affect OCV behavior. According to the OCV distribution results under high and low discharge test protocols during the battery's lifetime, OCV behaviors at 45 °C and 10 °C due to temperature and internal resistance (internal temperature) were smooth. However, neither environmental temperature nor internal resistance was enough at 25 °C to keep the OCV behavior smooth. Therefore, the OCV increased for the first 50~100 cycles and then stabilized. This was seen until the rate of the internal resistance increased and made the rate of the OCV stabilize.

5. Conclusions

This work discussed the control strategy of Li-ion batteries as the main component of EVs. Different battery management systems were addressed. Moreover, various methods for estimating the critical parameters of the battery, such as SoC, were introduced to understand the lifetime performance of the battery better.

A case study was investigated based on the OCV variation of the Li-ion battery at different ambient temperatures and three key SoC levels over the battery's lifespan. The results showed that changing the ambient temperature impacted the OCV variations of the battery. In other words, by increasing the temperature, the voltage fluctuation at 45 °C at low SOC of 50% and 20% was more significant than in other conditions. This issue impacts the BMS reliability and complicates the performance of the control strategy system task during the battery's lifetime.

In contrast, the rate of the OCV at different SoC in the low and high temperatures is more stable. Moreover, the outcome of the OCV investigation in different conditions showed the voltage behavior of the battery under high and low discharge test protocols during the battery's lifetime, and the OCV behaviors at 45 °C and 10 °C due to temperature and internal resistance (internal temperature) were smooth. However, neither environmental temperature nor internal resistance was enough at 25 °C to keep the OCV behavior smooth. The OCV rose for 50~100 cycles before stabilizing. This was seen until increasing internal resistance stabilized the OCV rate.

Author Contributions: F.H.G. planned the case studied, obtained the results writing—original draft preparation (Conceptualization and methodology); M.B. supervised the case studied (Supervision and investigation) and S.H.E.A.A. analyzed the results (writing—review and editing); F.H.G. and S.H.E.A.A. wrote the paper, which was further reviewed by A.E.-S. (validation), M.B., Z.M.A. (Zuhair M. Alaas) (formal analysis) and Z.M.A. (Ziad M. Ali) (final validation). All authors have read and agreed to the published version of the manuscript.

Funding: This research received no external funding.

Institutional Review Board Statement: Not applicable.

Informed Consent Statement: Not applicable.

Data Availability Statement: Not applicable.

Acknowledgments: We acknowledge the support of the research team from “Flanders Make”.

Conflicts of Interest: The authors declare no conflict of interest.

List of Abbreviations

BMS	Battery management system
C	Carbon
C-rate = 1C	Nominal output/input current of battery in one hour
EV	Electric vehicle
OCV	Open-circuit voltage
SoC	State of charge
SoE	Safe operating envelope
SoH	State of health
SoP	State of power
STPs	Standard test protocols
KF	Kalman filter
LFP	Lithium-Ion-Phosphate
Li-ion	Lithium-ion
Li-S	Lithium-Sulfur
LMO	Lithium-Ion Manganese Oxide
LTO	Lithium Titanium Oxide
NCA	Nickel-Cobalt-Aluminum-Oxide
NMC	Nickel-Manganese-Cobalt
V_{min}	Lower voltage safety limit
V_{max}	Upper voltage safety limit

References

1. Calasan, M.; Zobaa, A.F.; Hasanien, H.M.; Abdel Aleem, S.H.E.; Ali, Z.M. Towards accurate calculation of supercapacitor electrical variables in constant power applications using new analytical closed-form expressions. *J. Energy Storage* **2021**, *42*, 102998. [[CrossRef](#)]
2. Mostafa, M.H.; Abdel Aleem, S.H.E.; Ali, S.G.; Ali, Z.M.; Abdelaziz, A.Y. Techno-economic assessment of energy storage systems using annualized life cycle cost of storage (LCCOS) and levelized cost of energy (LCOE) metrics. *J. Energy Storage* **2020**, *29*, 101345. [[CrossRef](#)]
3. Gandoman, F.H.; Ahmed, E.M.; Ali, Z.M.; Berecibar, M.; Zobaa, A.F.; Abdel Aleem, S.H.E. Reliability evaluation of lithium-ion batteries for e-mobility applications from practical and technical perspectives: A case study. *Sustainability* **2021**, *13*, 11688. [[CrossRef](#)]
4. Ranieri, M.; Alberto, D.; Piret, H.; Cattin, V. Electronic module for the thermal monitoring of a Li-ion battery cell through the electrochemical impedance estimation. *Microelectron. Reliab.* **2017**, *79*, 410–415. [[CrossRef](#)]
5. Zhou, X.; Stein, J.L.; Ersal, T. Battery state of health monitoring by estimation of the number of cyclable Li-ions. *Control Eng. Pract.* **2017**, *66*, 51–63. [[CrossRef](#)]
6. Brunner, D.; Prasad, A.K.; Advani, S.G.; Peticolas, B.W. A robust cell voltage monitoring system for analysis and diagnosis of fuel cell or battery systems. *J. Power Sources* **2010**, *195*, 8006–8012. [[CrossRef](#)]
7. Wang, S.L.; Fernandez, C.; Zou, C.Y.; Yu, C.M.; Li, X.X.; Pei, S.J.; Xie, W. Open circuit voltage and state of charge relationship functional optimization for the working state monitoring of the aerial lithium-ion battery pack. *J. Clean. Prod.* **2018**, *198*, 1090–1104. [[CrossRef](#)]
8. Xie, S.; Ren, L.; Gong, Y.; Li, M.; Chen, X. Effect of Charging/Discharging Rate on the Thermal Runaway Characteristics of Lithium-Ion Batteries in Low Pressure. *J. Electrochem. Soc.* **2020**, *167*, 140503. [[CrossRef](#)]
9. Lu, Z.; Yu, X.; Zhang, L.; Meng, X.; Wei, L.; Jin, L. Experimental investigation on the charge-discharge performance of the commercial lithium-ion batteries. *Energy Procedia* **2017**, *143*, 21–26. [[CrossRef](#)]
10. Yu, Q.; Xiong, R.; Lin, C.; Shen, W.; Deng, J. Lithium-Ion Battery Parameters and State-of-Charge Joint Estimation Based on H-Infinity and Unscented Kalman Filters. *IEEE Trans. Veh. Technol.* **2017**, *66*, 8693–8701. [[CrossRef](#)]
11. Xiong, R.; Sun, F.; Gong, X.; He, H. Adaptive state of charge estimator for lithium-ion cells series battery pack in electric vehicles. *J. Power Sources* **2013**, *242*, 699–713. [[CrossRef](#)]
12. Xiong, R.; Sun, F.; He, H.; Nguyen, T.D. A data-driven adaptive state of charge and power capability joint estimator of lithium-ion polymer battery used in electric vehicles. *Energy* **2013**, *63*, 295–308. [[CrossRef](#)]

13. Lu, L.; Han, X.; Li, J.; Hua, J.; Ouyang, M. A review on the key issues for lithium-ion battery management in electric vehicles. *J. Power Sources* **2013**, *226*, 272–288. [[CrossRef](#)]
14. Hoque, M.M.; Hannan, M.A.; Mohamed, A.; Ayob, A. Battery charge equalization controller in electric vehicle applications: A review. *Renew. Sustain. Energy Rev.* **2017**, *75*, 1363–1385. [[CrossRef](#)]
15. Hannan, M.A.; Hoque, M.M.; Ker, P.J.; Begum, R.A.; Mohamed, A. Charge equalization controller algorithm for series-connected lithium-ion battery storage systems: Modeling and applications. *Energies* **2017**, *10*, 1390. [[CrossRef](#)]
16. Ju, F.; Deng, W.; Li, J. Performance Evaluation of Modularized Global Equalization System for Lithium-Ion Battery Packs. *IEEE Trans. Autom. Sci. Eng.* **2016**, *13*, 986–996. [[CrossRef](#)]
17. Wu, C.; Zhu, C.; Ge, Y. A New Fault Diagnosis and Prognosis Technology for High-Power Lithium-Ion Battery. *IEEE Trans. Plasma Sci.* **2017**, *45*, 1533–1538. [[CrossRef](#)]
18. Savari, G.F.; Krishnasamy, V.; Sathik, J.; Ali, Z.M.; Abdel Aleem, S.H.E. Internet of Things based real-time electric vehicle load forecasting and charging station recommendation. *ISA Trans.* **2020**, *97*, 431–447. [[CrossRef](#)]
19. Rawa, M.; Abusorrah, A.; Bassi, H.; Mekhilef, S.; Ali, Z.M.; Abdel Aleem, S.H.E.; Hasani, H.M.; Omar, A.I. Economical-technical-environmental operation of power networks with wind-solar-hydropower generation using analytic hierarchy process and improved grey wolf algorithm. *Ain Shams Eng. J.* **2021**, *12*, 2717–2734. [[CrossRef](#)]
20. Mohamed, N.; Aymen, F.; Ali, Z.M.; Zobaa, A.F.; Abdel Aleem, S.H.E. Efficient power management strategy of electric vehicles based hybrid renewable energy. *Sustainability* **2021**, *13*, 7351. [[CrossRef](#)]
21. Lyu, D.; Ren, B.; Li, S. Failure modes and mechanisms for rechargeable Lithium-based batteries: A state-of-the-art review. *Acta Mech.* **2019**, *230*, 701–727. [[CrossRef](#)]
22. Hu, X.; Zhang, K.; Liu, K.; Lin, X.; Dey, S.; Onori, S. Advanced Fault Diagnosis for Lithium-Ion Battery Systems: A Review of Fault Mechanisms, Fault Features, and Diagnosis Procedures. *IEEE Ind. Electron. Mag.* **2020**, *14*, 65–91. [[CrossRef](#)]
23. Chaoui, H.; Mandalapu, S. Comparative study of online open circuit voltage estimation techniques for state of charge estimation of lithium-ion batteries. *Batteries* **2017**, *3*, 12. [[CrossRef](#)]
24. Gandoman, F.H.; Jaguemont, J.; Goutam, S.; Gopalakrishnan, R.; Firouz, Y.; Kalogiannis, T.; Omar, N.; Van Mierlo, J. Concept of reliability and safety assessment of lithium-ion batteries in electric vehicles: Basics, progress, and challenges. *Appl. Energy* **2019**, *251*, 113343. [[CrossRef](#)]
25. Gandoman, F.H.; Van Mierlo, J.; Ahmadi, A.; Abdel Aleem, S.H.E.; Chauhan, K. Safety and reliability evaluation for electric vehicles in modern power system networks. In *Distributed Energy Resources in Microgrids: Integration, Challenges and Optimization*; Elsevier: Amsterdam, The Netherlands, 2019; pp. 389–404. ISBN 9780128177747.
26. Cheng, K.W.E.; Divakar, B.P.; Wu, H.; Ding, K.; Ho, H.F. Battery-management system (BMS) and SOC development for electrical vehicles. *IEEE Trans. Veh. Technol.* **2011**, *60*, 76–88. [[CrossRef](#)]
27. Lin, Q.; Wang, J.; Xiong, R.; Shen, W.; He, H. Towards a smarter battery management system: A critical review on optimal charging methods of lithium ion batteries. *Energy* **2019**, *183*, 220–234. [[CrossRef](#)]
28. Li, Y.; Chen, J.; Lan, F. Enhanced online model identification and state of charge estimation for lithium-ion battery under noise corrupted measurements by bias compensation recursive least squares. *J. Power Sources* **2020**, *456*, 227984. [[CrossRef](#)]
29. Li, X.; Huang, Z.; Tian, J.; Tian, Y. State-of-charge estimation tolerant of battery aging based on a physics-based model and an adaptive cubature Kalman filter. *Energy* **2021**, *220*, 119767. [[CrossRef](#)]
30. Li, S.; Li, Y.; Zhao, D.; Zhang, C. Adaptive state of charge estimation for lithium-ion batteries based on implementable fractional-order technology. *J. Energy Storage* **2020**, *32*, 101838. [[CrossRef](#)]
31. Liu, Z.; Qiu, Y.; Yang, C.; Ji, J.; Zhao, Z. A State of Charge Estimation Method for Lithium-Ion Battery Using PID Compensator-Based Adaptive Extended Kalman Filter. *Complexity* **2021**, *2021*, 115880. [[CrossRef](#)]
32. Omariba, Z.B.; Zhang, L.; Kang, H.; Sun, D. Parameter identification and state estimation of lithium-ion batteries for electric vehicles with vibration and temperature dynamics. *World Electr. Veh. J.* **2020**, *11*, 50. [[CrossRef](#)]
33. Tong, S.; Lacap, J.H.; Park, J.W. Battery state of charge estimation using a load-classifying neural network. *J. Energy Storage* **2016**, *7*, 236–243. [[CrossRef](#)]
34. Shen, P.; Ouyang, M.; Lu, L.; Li, J.; Feng, X. The co-estimation of state of charge, state of health, and state of function for lithium-ion batteries in electric vehicles. *IEEE Trans. Veh. Technol.* **2018**, *67*, 92–103. [[CrossRef](#)]
35. Meng, H.; Li, Y.F. A review on prognostics and health management (PHM) methods of lithium-ion batteries. *Renew. Sustain. Energy Rev.* **2019**, *116*, 109405. [[CrossRef](#)]
36. Khan, M.R.; Swierczynski, M.J.; Kær, S.K. Towards an ultimate battery thermal management system: A review. *Batteries* **2017**, *3*, 9. [[CrossRef](#)]
37. Liu, K.; Li, K.; Peng, Q.; Zhang, C. A brief review on key technologies in the battery management system of electric vehicles. *Front. Mech. Eng.* **2019**, *14*, 47–64. [[CrossRef](#)]